INFLUENCE OF ANNEALING AT 1100 ºC AND 475ºC ON THE MECHANICAL PROPERTIES AT ROOM TEMPERATURE OF PM2000 ODS ALLOY

J. Chao, J.L. González-Carrasco, C. Capdevila*

Department of Physical Metallurgy, Centro Nacional de Investigaciones Metalúrgicas (CENIM), Consejo Superior de Investigaciones Científicas (CSIC), Avda. Gregorio del Amo, 8, E-28040 Madrid, Spain

* Corresponding author. Tel.: +34-91-553-89-00; fax: +34-91-534-74-25.

E-mail address: ccm@cenim.csic.es (C. Capdevila)

Abstract

In the last few years the Fe-base oxide dispersion strengthened (ODS) PM 2000 alloy has been shown to be a biomaterial for its outstanding combination of mechanical properties and corrosion resistance. In this work, we are describing the effect of high temperature annealing at 1100 ºC (pre-oxidation) and low temperature annealing at 475ºC on the main mechanical properties at room temperature, with particular emphasis on tensile and fatigue properties, which are suitable for achieving the required biofunctionality of load bearing implants. It has been shown that annealing at 475 ºC is responsible for an increase in the YS and UTS with the subsequent decrease in ductility. However, despite of the loss of ductility, the material shows ductile behaviour as is observed in the necked zone of tensile specimens, which contrasts with the so-called "475 ºC embrittlement" observed for another ferritic alloys. Moreover, aged material at 475 ºC exhibits a better fatigue limit than that non aged pre-oxidised material.

Keywords: 475 ºC embrittlement, FeCrAl Oxide Dispersion Strengthened Alloy, Fatigue, Mechanical Properties

1. Introduction

PM 2000 (trademark of Plansee) is an ODS (oxide dispersion strengthened) Fe-20Cr-5Al alloy that combines an excellent oxidation resistance with reasonable creep strength; thus it is widely used for high temperature applications. Recently, the alloy has been investigated as potential biomaterial for surgical implants [1] owing to its ability for being coated in situ with a fine, dense and tightly adherent α-alumina layer by thermal oxidation at rather high temperature (pre-oxidation temperature of 1100 ºC), so combining the inherent mechanical properties of the substrate with the superior biocompatibility of the bulk alumina. The biocompatibility in vitro of the coated alloy has been found to be very promising [2,3]. It is suitable for the intended application because the elevated compressive residual stresses in the coating account for the ability to deform without cracking [3]. Information on its soft ferromagnetic properties can be found elsewhere [4].

Previous studies with MA 956, a similar FeCrAl ODS alloy, have reported a spinodal decomposition of the alloy into Fe-rich α and Cr-rich α`-phases during ageing at 475ºC [5,6]. Variations in the cooling rate from the pre-oxidation temperature, which yield different elapsed times around 475ºC, have shown that a decrease in the cooling rate causes an increase in the yield and tensile strength [7], and hardness [8]. Moreover, a ductile to brittle transition was observed at the lowest cooling rate which is consistent with the so-called "475ºC embrittlement" [7]. It is interesting to note that the absolute hardness increase during ageing of MA 956 for the recrystallized (coarse-grained) condition is higher than for the as-hot rolled (fine-grained) condition [9,10], irrespective of the processing route [9].

Likewise, the Pre-oxidation temperature is rather high (1100ºC) and, therefore, the microstructural changes could impair the good mechanical properties of the alloy at room temperature. Therefore, this investigation aims to investigate the effect of pre-oxidation at 1100 ºC and the 475ºC ageing of PM 2000 on the main mechanical properties, at room temperature, with particular emphasis on tensile and fatigue properties, which are necessary to achieve the required biofunctionality of load bearing implants [11]. To the author's knowledge, information on the effect of ageing on the fatigue behaviour has not been reported before. Computational tools will be used to evaluate the operating mechanism for hardening.

2. Materials and Experimental Techniques

The alloy under investigation, whose chemical composition (wt%) is 20 Cr, 5 Al, 0.5 Y_2O_3, bal. Fe, was prepared at Plansee Gmbh (Lechbruck, Germany) by a complex powder metallurgical (PM) route involving mechanical alloying and further consolidation of the powders to obtain a fully dense material. For this research a hot rolled bar of 35 mm in diameter was prepared. Test samples were removed from the bar by electrospark erosion, then machined to the final shape. Grinding of the specimens was performed with successively finer silicon carbide papers followed by polishing with diamond paste. Finally, the specimens were washed in running water and then cleaned with alcohol.

Pre-oxidation treatment, aimed at generating the outer alumina layer, was performed at 1100ºC for 120 h in air, followed by slow furnace cooling to room temperature. These experimental conditions were selected as the most suitable to obtain a dense and adherent α-Al_2O_3 scale [1]. To investigate the influence of the scale on the mechanical properties, a set of specimens were machined from a bar which was heat treated under

the conditions used for pre-oxidation. Therefore, these specimens have the same microstructure as the specimens with scale. Unless otherwise stated, the materials will be referred to as specimens with scale (heat treatment after the specimen preparation) and scale-free specimens (heat treatment before machining of the specimen). To assess the effect of ageing at 475ºC, a set of specimens of both material conditions were annealed for several exposures at this temperature.

The mechanical properties were evaluated by tests of Vickers hardness, tensile, and rotating bending fatigue. Vickers hardness of polished samples was measured on a cross section perpendicular to the longitudinal bar direction. Indentations were made with 1-kgf load and 15-seconds dwell time. At least eight measurements were made on each sample. The tensile specimens had a gauge length of 45 mm and 8 mm in diameter. The samples were tested at room temperature using two strain rates, namely 5.10^{-2} s^{-1} and 5.10^{-5} s^{-1}. At least two tests were conducted on any given material condition. The Young modulus, the 0.2-pct yield strength, the tensile strength, and the tensile elongation were evaluated from the stress/strain curves.

The fatigue strength at 10^8 cycles was estimated from the data obtained by rotating bending tests (R=-1). Specimens were subjected to a constant amplitude loading at 300 Hz. Un-notched hourglass-shaped fatigue specimens with a 5.885 mm diameter waist and 80 mm in length were used. Once machined, these specimens were polished with successively finer silicon carbide and polished along the longitudinal direction with 1 μm diamond paste. In order to evaluate the notch effect and surface finish of machining on fatigue strength a U-notch of 1.75 mm in depth and a notch tip radius of 0.875 mm was ground using normal workshop practice on cylinders of 10 mm diameter and 80 mm in length. In this case no finishing operations were performed on the specimens. This notch geometry was chosen in order to provide oxide scale integrity at the notch tip. This notch resulted in a stress concentration factor of 1.86 [12]. Because of the small

differences in the machining of the notch, the stress concentration factor ranged between 1.85 and 1.87.

Optical and scanning electron microscopy (SEM)was used for the microstructural analysis and examination of the fracture surfaces and in order to obtain a higher resolution a scanning electron microscope equipped with a field emission gun was used. Depending on the analysis, secondary (SEI) or backscattered electron images (BEI) were selected. From the SEI images obtained under 5000 times magnification of longitudinal sections of unbroken specimens the surface roughness of both pre-annealed and notched specimens was estimated

3. Results

In the as-received condition, the material presents a weak <110> fibber texture and a very elongated and fibrous structure, as it can be seen in OM image of Fig. 1. At higher magnifications, Fig. 2, it can be seen from the backscattered image of the figure that the microstructure consists of grains of about 1 μm in diameter that are elongated in the longitudinal bar direction. Following the pre-oxidation treatment the texture does not vary significantly, the grain size grows slightly but still remain elongated. On the other hand, the pre-oxidation treatment generates a tightly adherent α-alumina scale between 3-4 μm thick, as it is shown in the SEM image of Fig.3, which is consistent with the temperature and exposure times used for pre-oxidation [13]. In addition, beneath the oxide scale a uniform layer of recrystallised material with a thickness of about 10 microns was found (as it is shown in the backscattered image of Fig.4), although occasionally surface patches of recrystallised material of about 500 μm in depth could

be observed. Grains of this region were orientated towards the <110> direction or with the <111> direction parallel to the longitudinal axis of the bar.

The ageing treatment at 475ºC for 100 hours produces a hardening effect. According with previously reported results ins MA956 [5,6], and bearing in mind the similar chemical composition between PM2000 and MA956, this phenomenon could be explained by a nanometric scale decomposition of the supersaturated solid solution into Fe-rich α and Cr-rich α' phases, as it would be theoretically demonstrated in the next paragraphs.

In the following sections, the influence of ageing at 475ºC on specimens with and without scale on their mechanical properties at room temperature is described. The whole set of data is summarised in Table I.

3.1 Hardness

Hardness measurements show a relative hardness decrease after the pre-oxidation treatment from 300 to 287 HV, which is associated with the moderated grain growth and annihilation of microstructural defects. After ageing at 475ºC, the as-received and pre-oxidised specimens experience a significant hardening from the shortest period of testing, Fig. 5. No significant differences in the hardness increase for a given ageing time was observed between both material conditions.

3.2 Tensile Tests

The Young's modulus of the material disregarding the material state was 170±10 GPa. With regards to the tensile properties in the as-received condition, pre-annealing of PM

2000 at the oxidation temperature causes a slight decrease in the yield (about 6%) and tensile (about 1%) strengths, and an increase (50%) in the ductility, Table I. The moderate decrease in the tensile properties provides evidence of the high stability of the microstructure during pre-oxidation. The tensile properties of pre-oxidised specimens (with scale) are similar to those obtained for the alloy pre-annealed at the oxidation temperature (scale free). These results, therefore, indicate that neither the oxide scale nor the under layer of recrystallised material affect the tensile behaviour significantly. Thus, the ageing effect was only considered for the pre-oxidised specimens, i.e. samples with scale.

Ageing of the pre-oxidised specimens at 475ºC for 100 h causes a significant increase in both yield and tensile strengths, with the concomitant decrease in elongation. An increase in the strain rate for pre-oxidised and pre-oxidised plus aged tensile specimens produces an increase in the yield and tensile strengths without significant changes in the elongation.

The macroscopic appearance of the fracture surface, Fig. 6, indicates a strong area reduction and a typical “cup-cone” fracture, which agree with the large elongation values. In the case of the specimens tested at the highest strain rate, the shape of the necking is rather asymmetric. It is interesting to note that the fracture surface of specimens tested at the lowest strain rate shows splitting that does not greatly affect either the elongation or the area reduction values. FEG/SEM micrographs of the surface of delaminations, Fig. 7, indicate that the material separation runs along the fibres by almost an intergranular mode with some tear ridges. From the macroscopic aspect of the fracture surface of the aged material, Fig. 8, it can be seen that delamination radiates from the ductile tear at the specimen centre. Two relevant conclusions arise from these observations. Firstly, splitting could be a diffusion-controlled process, presumably due to hydrogen embrittlement, since it was found to be sensitive to the strain rate. Secondly,

the longitudinal embrittlement does not affect the tensile properties. These aspects should be treated in a further work.

3.3 Rotating bending fatigue tests

The estimated surface roughness (Ra) of the annealed (polished) and notched (ground) specimens were about 0.5 μm and 1.3 μm, respectively. The figures 9-11 show plots of the stress amplitude versus cycles number of cycles to failure for the conditions under investigation. From the analysis of these figures, the role of the annealing, oxide scale, notch and ageing can be envisaged. The fatigue limit estimated from these plots is also tabulated in Table I. As can be seen, Fig. 9, the annealing treatment produces a decrease of about 40 MPa in the fatigue limit with regards to the as-received material (fine grained). As regards the annealed material, no effect of the oxide scale on the fatigue limit is observed. Fig. 10 shows that the ageing treatment increases the fatigue limit of pre-annealed and pre-oxidised material, the increase being lower in the latter case. The combination of notch and machining factors produces a decreasing in the fatigue limit of the as-received material, Fig. 11. However, the magnitude of this decrease is lower than the ratio of the fatigue limit of un-notched specimens upon the stress concentration factor. The aging treatment does not produce an appreciable improvement in the fatigue limit.

4. Discussion

A theoretical study of the α and α' distribution has been carried out in PM2000. The thermodynamic calculations involved here have been performed using the commercial

software package, MTDATA [14]. Calculations revealed that Al-content affects the presence or absence of σ-phase in the microstructure. Since this precipitation could also cause a hardening, the evolution of the α' and σ phase for different Al-contents has been analysed. Fig. 12 shows the evolution of the α and σ-phase in the Fe-Cr-Al system for Al content ranging from 0 to 6 wt.-%. It is clear from this figure that the σ-phase is not predicted for the studied alloy. Hence, the hardening effect could be caused by spinodal decomposition. Finally, Fig. 13 shows the Cr distribution in α'-phase with temperature. It is worth noting that an Al-content increase leads to an increase in the amount of Cr which is located in the α'-phase. With regards to the precise strengthening mechanism, a simultaneous effect of the misfit in the coherent internal stresses and the spatial variation of the Young modulus is likely to occur [15].

Somewhat surprising is the fact that hardness increase for the as-received and pre-annealed specimens, Fig.5, is rather similar, which contrasts with previous results for MA 956 alloy where hardness increase was much higher for the pre-annealed condition [9,10]. Microstructural comparison between both alloys reveals that recrystallisation of MA 956 during annealing at 1100ºC produces a severe grain growth, of up about 150 μm, and a change in the fibber texture from <110> to <100> [16]. The relation of these microstructural differences with the different hardening behaviour is uncertain since microstructural factors should not influence spinodal decomposition.

With regards to the tensile behaviour, the increase in hardness after ageing is accompanied by an increase in the yield and tensile strength and by a decrease in the ductility, which is consistent with previous results for MA 956 [7]. Despite the loss of ductility, the material exhibits ductile behaviour as is shown in the necked zone of tensile specimens. This ductile behaviour contrast with the so-called "475ºC embrittlement" observed for other aged ferritic alloys [17]. As a matter of fact, MA956 exhibits brittle behaviour when testing under similar conditions [7] that can be

explained by the recrystallization of the material. Effectively, as is well known the ferritic alloys experience a ductile-brittle transition (DBT) at a temperature that depends on the grain size, strain rate, and stress triaxiality [18]. Therefore, the effect of ageing at 475ºC is to produce an increase in the yield strength that facilitates the achievement of the cleavage stress characteristic yielding to a brittle behaviour. Such an effect is similar to the effects on the DBT of a temperature decrease and the increase in both, the strain rate and stress triaxiality. The ductile behaviour observed for PM 2000, with regards to that of MA956 [7] could be therefore attributed to its smaller grain size (2 μm versus 150 μm, respectively). Moreover, considering the effect of the texture on the DBT temperature for MA956 alloy [19], the <110> fibber texture determined for the PM 2000 investigated in the present work would be less favourable for embrittlement than that of the <100> fibber texture reported for the recrystallised MA956 alloy [7].

The fatigue behaviour of structural components is strongly affected by the presence of notches or section changes and by the surface state, i.e. the surface finish and the material properties in the near-surface zone. Nucleation of fatigue cracks is usually preceded by the formation of persistent slip bands that emerge to the free surface and act as notches. Therefore, any change in the surface state during fabrication or service modifies the fatigue behaviour. Regarding the pre-annealed (without scale) material, the oxidised alloy presents the following features that could modify the fatigue behaviour. Firstly, the initial surface state is removed upon heating to 1100ºC. Secondly, Al_2O_3 scale of about 5 μm thickness is generated at the above temperature during 100 h. Moreover, during oxidation the region of the substrate below the scale is plastically deformed because of the growth stresses. Additionally, a recrystallisation of a thin region of the substrate below scale takes place which produces an increase in the grain size and a texture change from a weak <110> fibre texture of the substrate to that of grains with the <111> direction or the <110> direction in the longitudinal sense of the

bar [19]. Upon cooling to room temperature the oxide scale and presumably the recrystallised/deformed region of the substrate become highly compressed and the remaining substrate slightly tensioned because of the mismatch of the thermal expansion coefficients. The magnitude of the stresses in the scale is about 4 GPa [16]. The oxide scale is well adhered to the substrate and presents some isolated pores without signs of spallation. Because of these features of the scale, it could be expected that during fatigue test, the scale locks the egress of mobile dislocations, delaying the nucleation of the fatigue cracks. Once the scale cracking takes place, the stress relaxation in the scale would produce first a delamination and then a spallation of the scale [20]. Therefore, the scale cracking would lose the protective capacity but would not enhance the crack propagation through the substrate. Regarding the annealed material, fatigue behaviour of the oxidised material, in which scale spallation has occurred, should be expected to be different enough because of the very different surface state. The first difference concerns a sample size effect, associated with the lower surface area susceptible to localised deformation. The annealed material shows a smooth surface, while a rough surface was generated during oxidation of the material. The magnitude of the surface residual stress should also be different. While in the oxidised material, a thin region of the substrate (the plastically deformed region during oxidation) could be highly compressive, in the polished samples of the pre-annealed material, negligible surface compression stresses should be expected. On the other hand, grain size of the material below the oxide scale is higher than that of the annealed material or equivalently than that of the oxidised samples below the recrystallised zone. Therefore, as the resistance to initiation of a slip band decreases with increasing grain size, the resistance to fatigue nucleation should be lower in the oxidised cracked material. However, the effect of grain size on cyclic plastic deformation is lower than that of monotonic plastic deformation [21]. Furthermore, it is also necessary to take into

account the variation of the crystalline orientation of the grains in the surface of the oxidised material, with regards to those corresponding to the annealed material. The microstructure of the recrystallised region, Fig. 4, consists of a string of grains, ones with the <111> direction parallel to the longitudinal direction of the bar and ones with the <110> direction parallel to the longitudinal direction. This feature could produce an additional size effect because, in regard to the applied stress, the <111> orientation of grains are less favourable to yielding than those of the texture components of the annealed material. In spite of the above considered scale-related effects and the surface and subsurface state of the annealed and oxidised materials great differences in their fatigue behaviour are not appreciable, Fig. 9. Two possible reasons could be the cause of this behaviour. Firstly, that the oxide scale was cracked. Secondly, the negative effects of a higher grain size and of the surface roughness of oxidised specimens could be offset by a higher magnitude of the surface residual stresses and the sampling effects above mentioned.

Now, we will consider the effect of aging on the fatigue behaviour, Fig. 10. The results of Fig. 10a shows that aging produces a notable increase in the endurance limit respect to that un-aged of pre-annealed material. The fatigue ratio (ratio of fatigue strength to tensile strength for 10^7 cycles) ranges from 0.4 for high strength steels to 0.6 for low and medium strength steels [22]. It could be considered this parameter as a qualitative measure of the propensity to plastic strain localization and/or of the plastic strain magnitude needed to crack nucleation. In the last row of Table I the fatigue ratio values for each condition of the material here considered are given. It can be noted a sensible decrease from 0.545 of the annealed material to that of 0.519 of annealed and aged material. Therefore, the aging treatment produces not only an increase in the endurance limit but also a higher propensity to the elastic strain localization to crack nucleation. Because of the uniformity of the phenomenon occurring during aging, it should be

expected a decrease of the plastic strain magnitude to crack nucleation instead of the observed enhanced propensity to plastic strain localization. It is also important to note that in the case of the material in the oxidised state the effect of aging is still more pronounced.

4. Conclusions

1.- Aging treatment at 475 ºC for 100 h produces an increase in the YS and UTS with the subsequent decrease in ductility. However, despite the loss of ductility, the material exhibits ductile behaviour as is observed in the necked zone of tensile specimens, which contrast with the so-called "475 ºC embrittlement" observed for other ferritic alloys.

2.- Surprisingly, similar fatigue results between annealed and oxidised samples are obtained in spite of the a priori very different scale related effects, the sub-surface state, grain size near the surface, and the surface roughness.

3.- In absolute terms, the aged material exhibits a better endurance limit that that unaged material. However, the lower value of fatigue ratio of aged material indicates a higher sensitivity to fatigue damage.

References

[1]G. Ciapetti, J.L. González-Carrasco, L. Savarino, M.A. Montealegre, S. Pagani and N. Baldini: Development of alumina forming ODS ferritic superalloys as new biomaterials for surgical implants (ALUSI), Growth Programme: GRD1-1999-10659, EU, Bruxells, (2000), 1.

[2] G. Ciapetti, J.L. González-Carrasco, L. Savarino, M.A. Montealegre, S. Pagani and N. Baldini: Biomaterials, 26 (2005), 849.

[3] J.L. González-Carrasco, G. Ciapetti, M.A. Montealegre, S. Pagani, J. Chao and N. Baldini: Biomaterials, 26 (2005), 3861.

[4] M.S. Flores, G. Ciapetti, J.L. González-Carrasco, M.A. Montealegre, M. Multigner, S. Pagani and G. Rivero: J. Mat. Sci.: Materials in Medicine, 15 (2004), 1.

[5] H.G. Read and H. Murakami: Appl. Surf. Sci., 94-95 (1996), 334.

[6] H.G. Read, H. Murakami and K. Hono: Scr. Mater., 36 (1997) 355.

[7] J. Chao and J.L. González-Carrasco: Mater. Sci. Technol., 14 (1998), 440.

[8] J. Chao and J.L.González-Carrasco: Metall. Mater. Trans. A, 34A (2003), 2681.

[9] J. Chao and J.L. González Carrasco: Scr. Mater., 47 (2002), 423.

[10] J. Chao and J.L. González-Carrasco: Scr. Mater., 49 (2004), 1457.

[11] D.F. Williams: Medical and Dental Materials, ed. by D.F. Williams, Materials Science and Technology, Weinheim, (1991), 1.

[12] R.E. Peterson: Stress concentration design factors, John Wiley, New York, (1973), 210.

[13] G. Strehl, J.L. González-Carrasco, J.L. Peris, M.A. Montealegre, S. García, C. Atienza and G. Borchardt: Surface and Coating Technology, 2006, in Press.

[14] Metallurgical and Thermochemical Databank, National Physical Laboratory, Teddington, (1996), 1.

[15] M. Kato: Acta Metall., 29 (1981), 79.

[16] J. Chao, J.L. González-Carrasco, J. Ibañez, M.L. Escudero and G. González-Doncel: Metall. Mater. Trans. A, 27A (1996), 3809.

[17] P.J. Grobner: Metall. Trans., 4 (1973), 251.

[18] G.T Hahn: Metall. Trans. A, 15A (1984), 947.

[19] J. Chao and J.L. González-Carrasco: Proc. of VII Congreso Propiedades Mecánicas de Sólidos, Universidad Politécnica Valencia, Valencia, (2002), 385..

[20] H.E. Evans: Mater. Sci. Eng. A, A120 (1989), 139.

[21] P. Lukas and L. Kunz: The Johannes Weertman Symposium, ed. by R.J. Arsenault, D. Cole, T. Gross, G. Kostorz, P.K. Liaw, S. Parameswaran, H. Sizek,The Mineral Metals & Materials Society, Warrendale, 1996, pp. 279-290.

[22] K-H. Park, J.C. LaSalle, L.H. Scwartz and M. Kato: Acta Metall. 34 (1986), 1853.

Figure Captions

Figure 1. Optical micrograph of the as-received material. X1000.

Figure 2. Backscattered electron image revealing the microstructure of the as-received material. A) Longitudinal section. B) Transverse section

Figure 3. Secondary electron image of a transverse section showing the oxide scale.

Figure 4. . Backscattered electron image revealing the recrystallised region beneath the oxide scale

Figure 5 Hardness increase as a function of ageing time at 475ºC

Figure 6. Optical photographs showing the necking features of preoxidised tensile specimens. A) Unaged specimens (1) $\varepsilon=5.10^{-5}s^{-1}$, (2) $\varepsilon=5.10^{-2}s^{-1}$. B) Aged specimens (1) $\varepsilon=5.10^{-5}s^{-1}$, (2) $\varepsilon=5.10^{-2}s^{-1}$.

Figure 7. SEM micrographs indicating (A) the path along of microstructure and (B) the surface aspect.

Figures 8 (A) Optical photograph showing the splitting and (B) SEM micrograph showing as splitting starts from the ductile crack in a tensile specimen of the preoxidised samples aged at 475ºC.

Figure 9 S-N diagram for PM 2000 in the as-received, pre-annealed y pre-oxidised conditions. The arrows indicate that tests were interrupted without failure of the specimen.

Figure 10 S-N diagram for (A) pre-annealed and (B) pre-oxidised specimens with and without ageing at 475ºC for 100 h. The arrows indicate that test was interrupted without failure of the specimen.

Figure 11 S-N diagram for as-received specimens with and without notching aged at 475ºC for 100 h. The arrows indicate that test was interrupted without failure of the specimen.

Figure 12.- (A) α' and (B) σ phase evolution with temperature.

Figure 13.- Fraction of Cr in α' phase as a function of temperature.

Table I. Tensile and fatigue properties of investigated conditions for PM 2000.

		As-received	Annealed at 1100ºC/120h			
			(scale free)		(with scale)	
Parameter	Strain rate (s^{-1})		Un-aged	Aged (475ºC/100h)	Un-aged	Aged (475ºC/100h)
Yield Strength (MPa)	5×10^{-5}	770	744	951	741	940
	5×10^{-2}	790	775	1040	775	1011
Tensile Strength (MPa)	5×10^{-5}	916	913	1067	930	1062
	5×10^{-2}	925	921	1130	954	1112
Elongation ($L_o=5d_o$) %	5×10^{-5}	19	23.5	19	24	19.8
	5×10^{-2}	16	21	17	22.5	18.4
Area Reduction (%)	5×10^{-5}	66.4	70	62	69.5	60.5
	5×10^{-2}	63.2	69.2	60	69	61
Fatigue Strength at 10^8 cycles (MPa)	--	320	500	570	500	530
Fatigue Strength/ Tensile strength	--	0.586	0.545	0.519	0.531	0.487

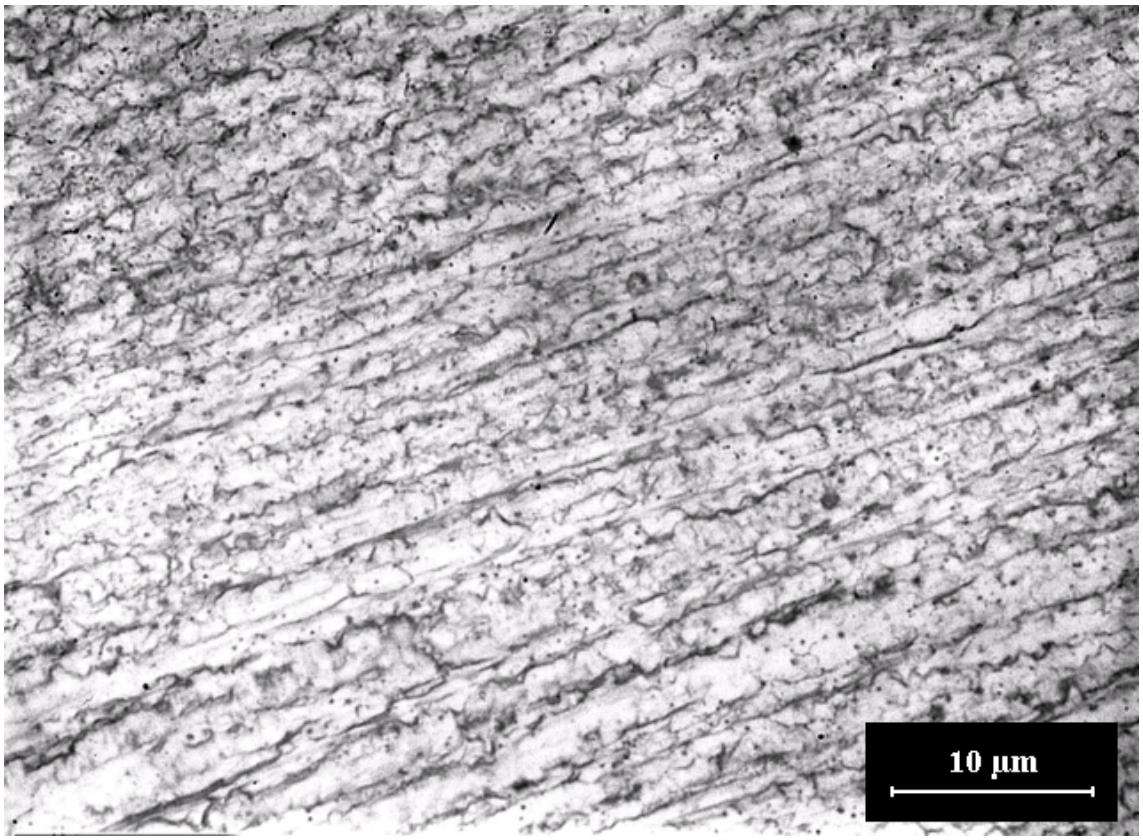

Figure 1. Optical micrograph of the as-received material. X1000.

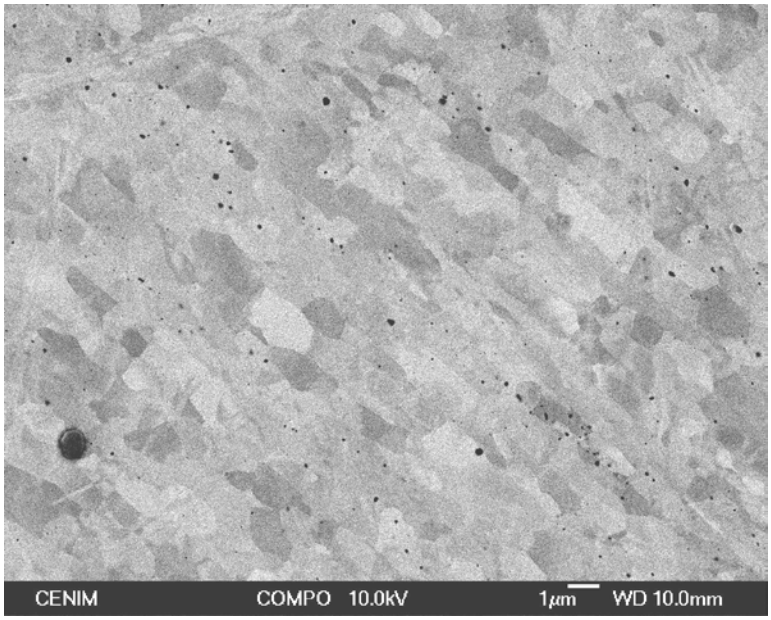

(A)

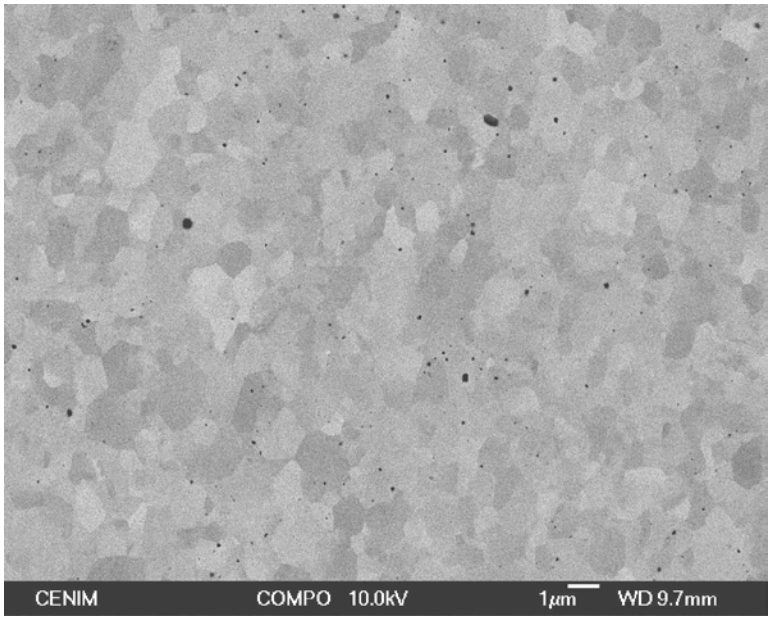

(B)

Figure 2. Backscattered electron image revealing the microstructure of the as-received material. A) Longitudinal section. B) Transverse section

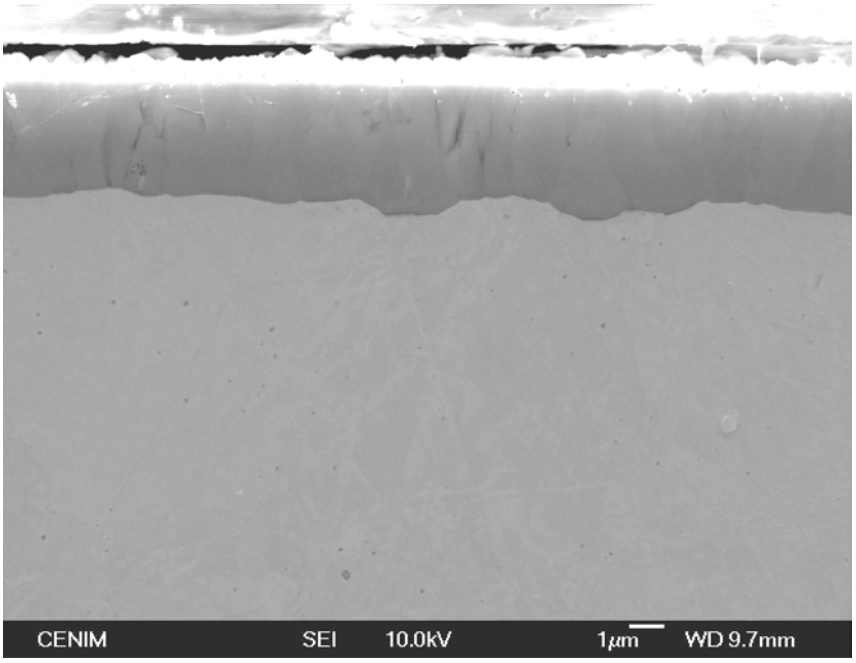

Figure 3. Secondary electron image of a transverse section showing the oxide scale.

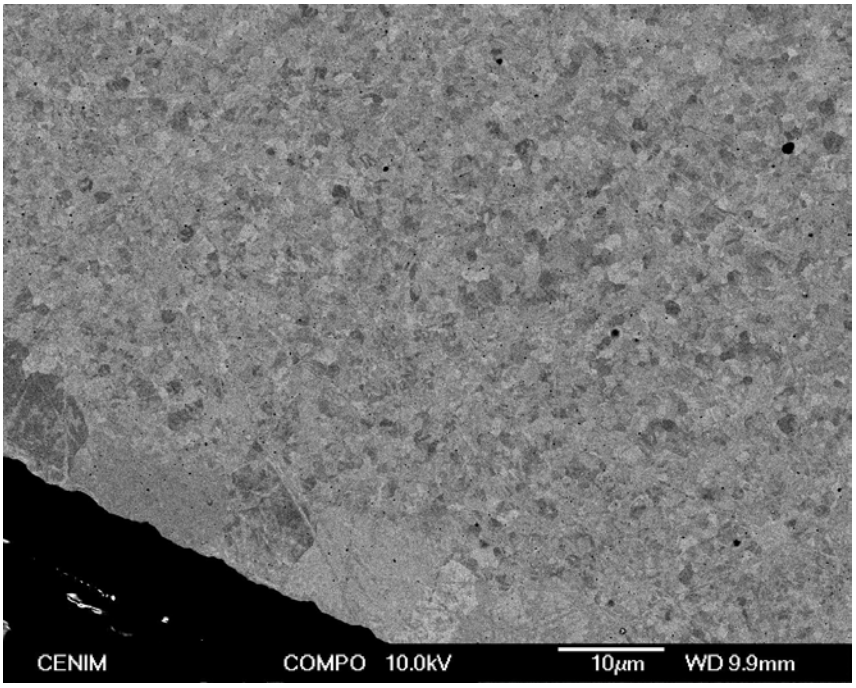

Figure 4. . Backscattered electron image revealing the recrystallised region beneath the oxide scale

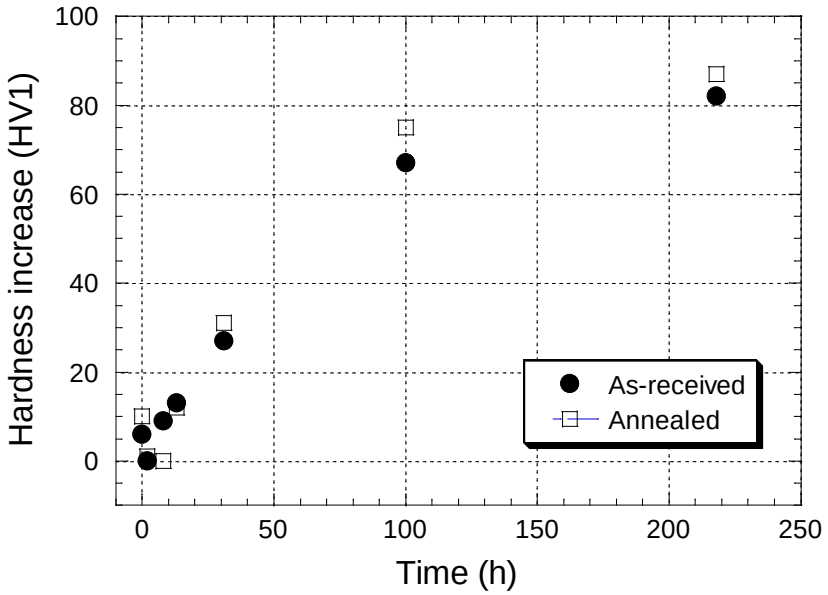

Figure 5 Hardness increase as a function of ageing time at 475ºC

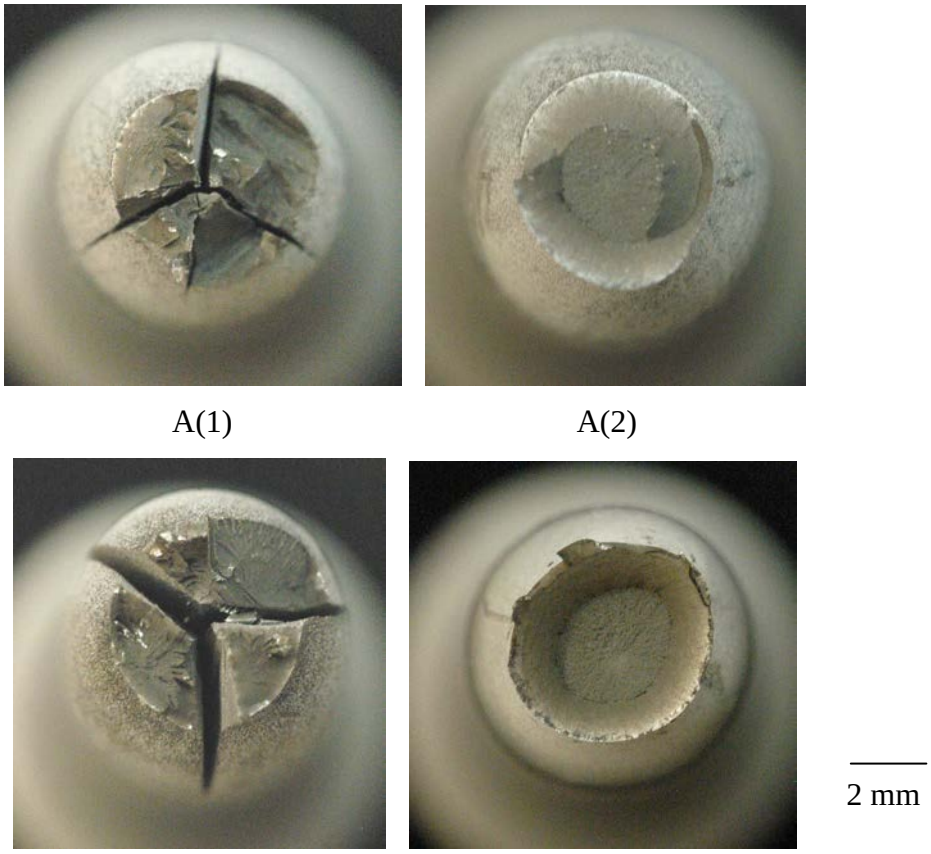

Figure 6. Optical photographs showing the necking features of preoxidised tensile specimens. A) Unaged specimens (1) $\dot{\varepsilon}=5.10^{-5}s^{-1}$, (2) $\dot{\varepsilon}=5.10^{-2}s^{-1}$. B) Aged specimens (1) $\dot{\varepsilon}=5.10^{-5}s^{-1}$, (2) $\dot{\varepsilon}=5.10^{-2}s^{-1}$.

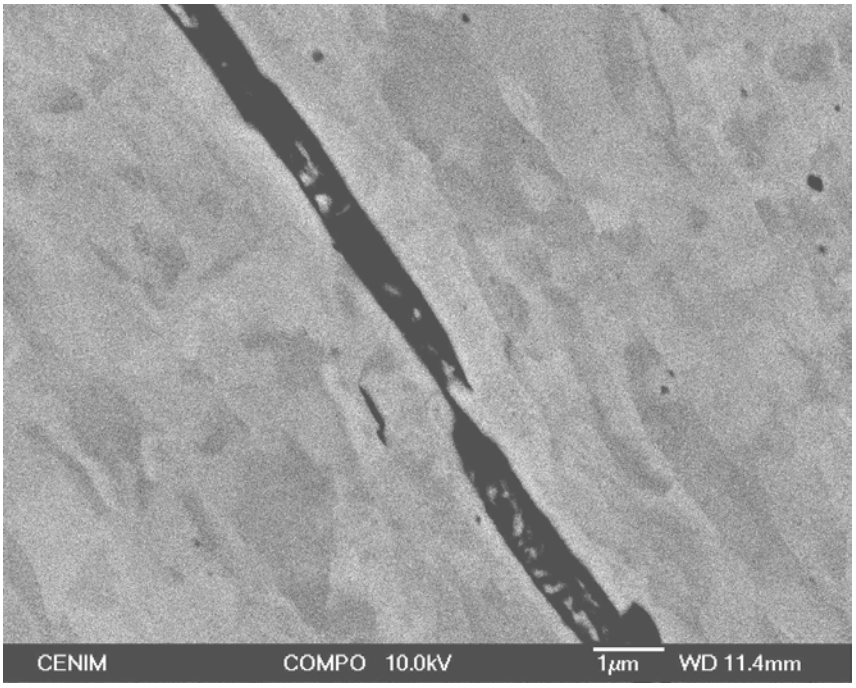

(A)

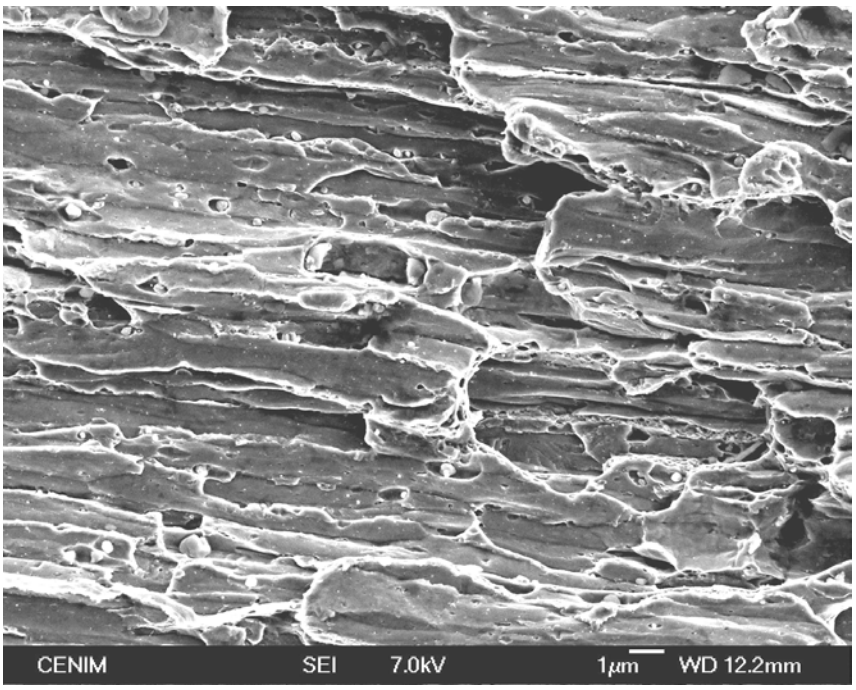

(B)

Figure 7. SEM micrographs indicating (A) the path along of microstructure and (B) the surface aspect.

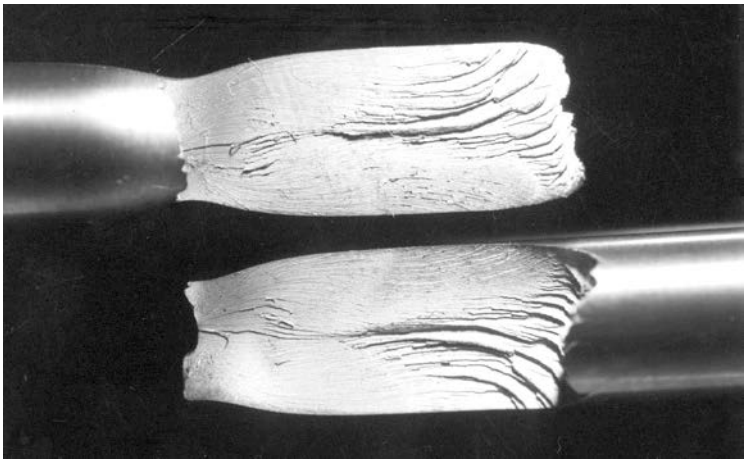

(A)

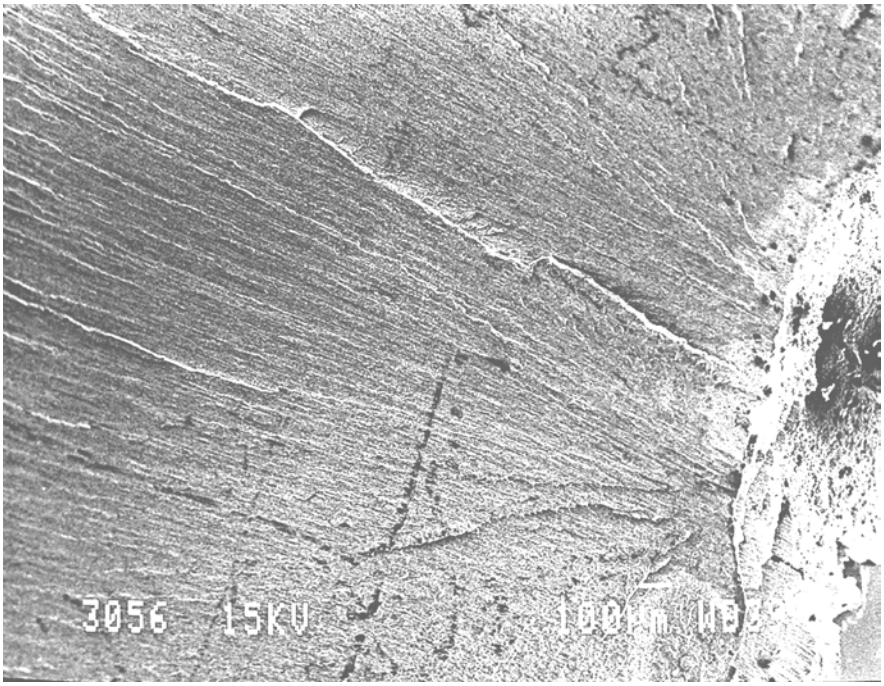

(B)

Figures 8 (A) Optical photograph showing the splitting and (B) SEM micrograph showing as splitting starts from the ductile crack in a tensile specimen of the preoxidised samples aged at 475ºC.

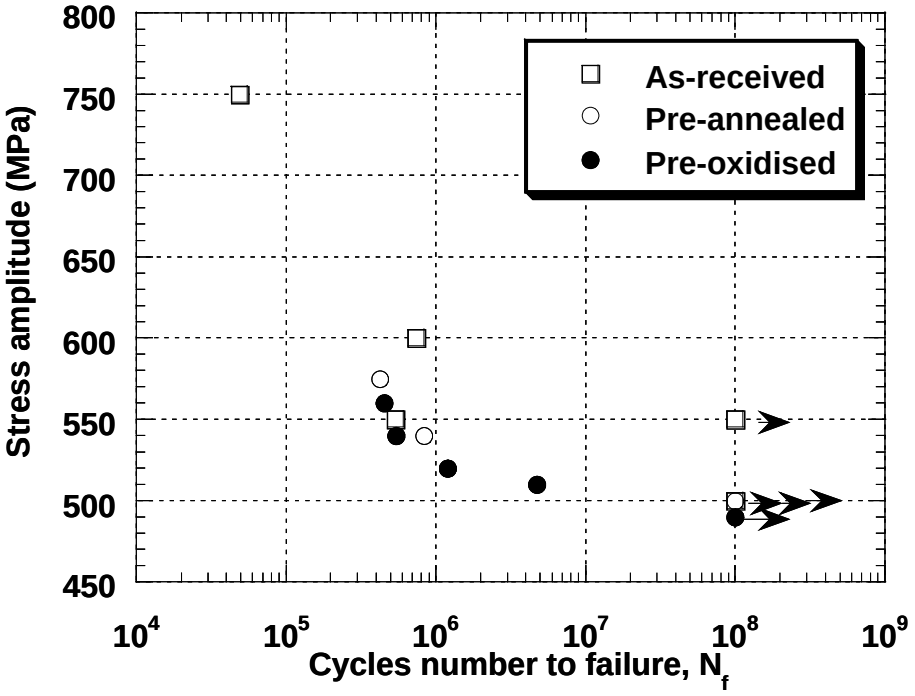

Figure 9 S-N diagram for PM 2000 in the as-received, pre-annealed y pre-oxidised conditions. The arrows indicate that tests were interrupted without failure of the specimen.

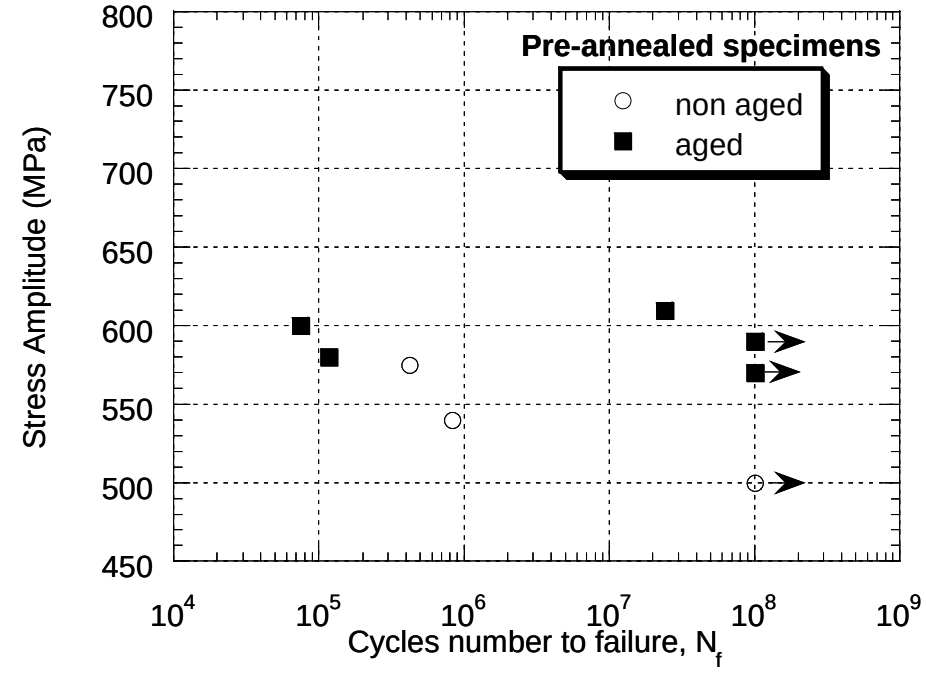

(A)

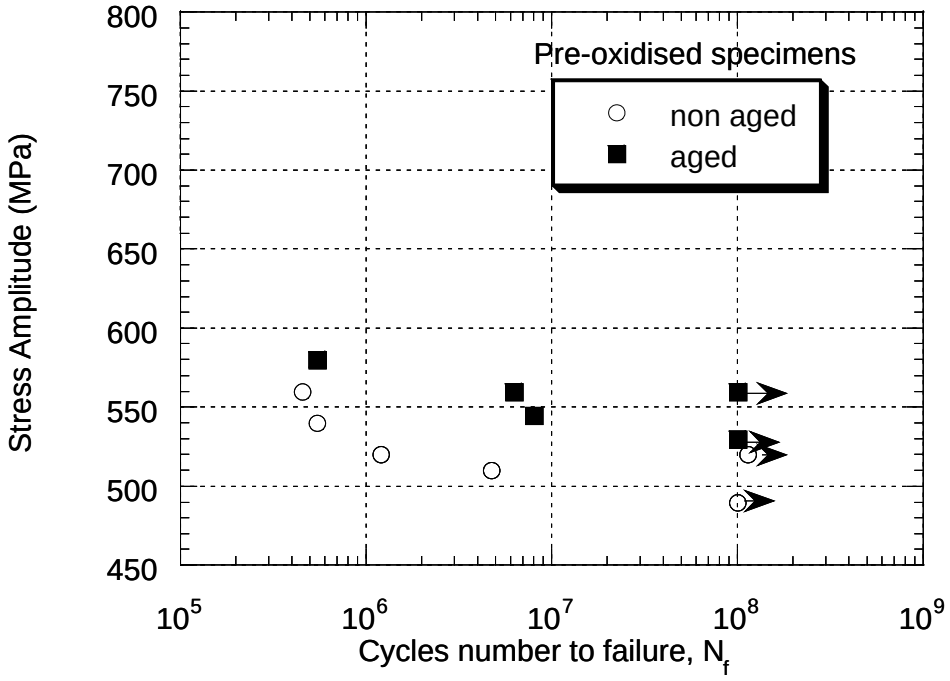

(B)

Figure 10 S-N diagram for A) pre-annealed and B) pre-oxidised specimens with and without ageing at 475ºC for 100 h. The arrows indicate that test was interrupted without failure of the specimen.

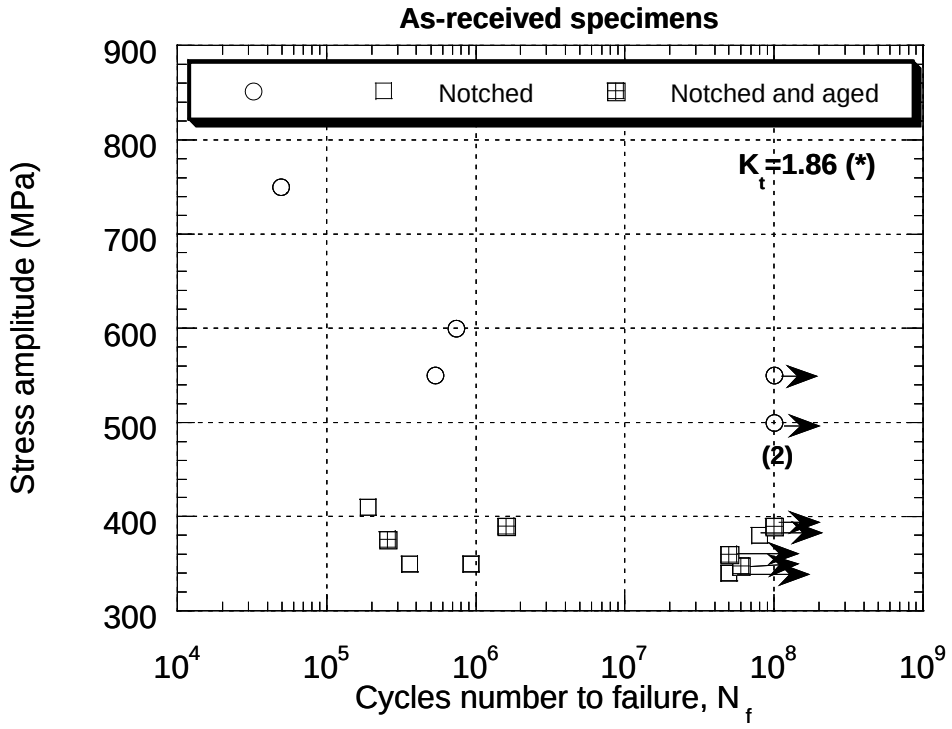

Figure 11 S-N diagram for as-received specimens with and without notching aged at 475ºC for 100 h. The arrows indicate that test was interrupted without failure of the specimen.

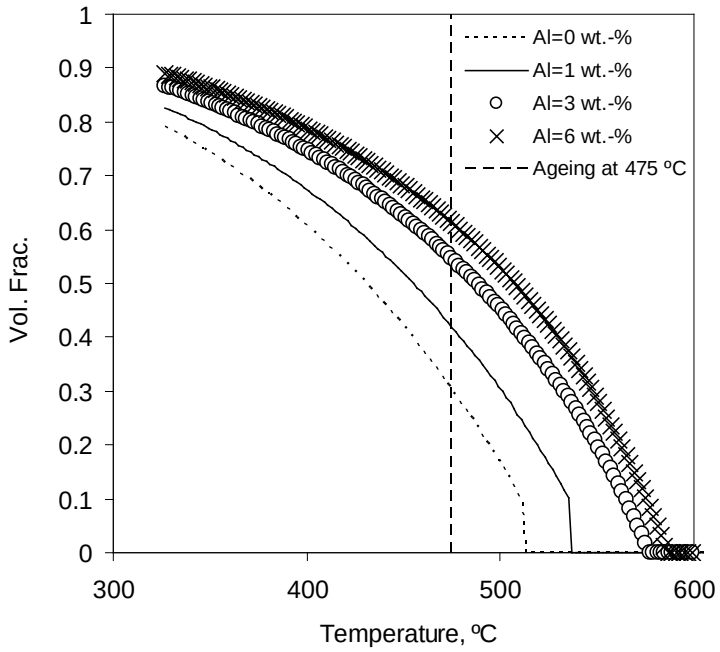

(A)

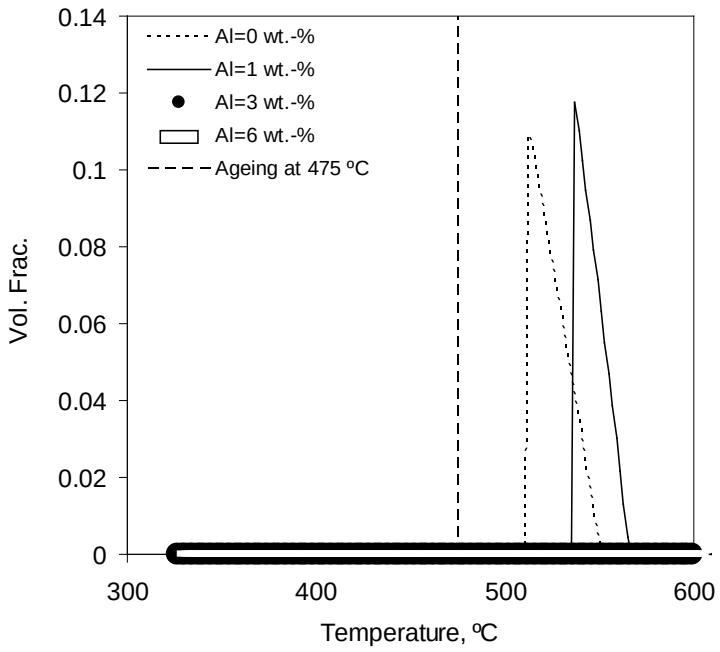

(B)

Figure 12.- (A) α' and (B) σ-phase evolution with temperature.

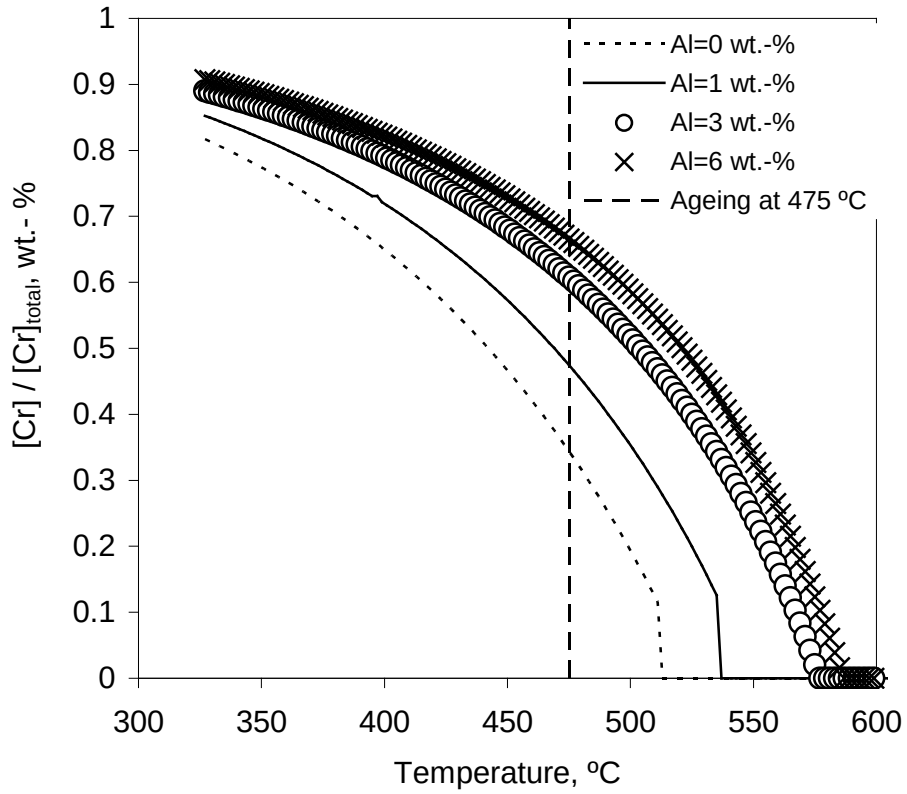

Figure 13.- Fraction of Cr in α'-phase as a function of temperature.